

Received April 5, 2020, accepted April 27, 2020, date of publication May 6, 2020, date of current version May 20, 2020.

Digital Object Identifier 10.1109/ACCESS.2020.2992506

Load Identification and Deflection Monitoring of Opening Beam on Well-Hole Freight Trains

YITONG WU^{1,2,3,4}, XIFENG LIANG^{1,2,3,4}, WEI ZHOU^{1,2,3,4}, LIN CHEN^{1,2,3,4},
JIE HE⁵, XIWEN GUO⁶, AND QIANXUAN WANG⁷

¹School of Traffic and Transportation Engineering, Central South University, Changsha 410075, China

²Key Laboratory of Traffic Safety on Track, Ministry of Education, Central South University, Changsha 410075, China

³Joint International Research Laboratory of Key Technology for Rail Traffic Safety, Central South University, Changsha 410075, China

⁴National and Local Joint Engineering Research Center of Safety Technology for Rail Vehicle, Changsha 410075, China.

⁵China State Railway Group Company, Ltd., Beijing 100844, China

⁶China Special Article Logistics Corporation, Ltd., Beijing 100070, China

⁷School of Railway Tracks and Transportation, Wuyi University, Jiangmen 529020, China

Corresponding author: Wei Zhou (zhou_wei000@126.com)

This work was supported in part by the National Key Research and Development Program of China under Grant 2017YFB1201201, and in part by the 2020 Special Funds for the Cultivation of Guangdong College Students' Scientific and Technological Innovation (Climbing Program Special Funds) under Grant pdjh2020a0592.

ABSTRACT In railway freight transport of over-size cargos, elastic deflection of overloaded structures is the main cause of train-line collision in running. Deflection monitoring remains a challenge for the non-uniform and opening beam on well-hole freight cars. This work presented a new approach by strain perception and Finite Element Analysis (FEA). In theoretical modeling, support locations and the geometry symmetry were taken into account, to identify the support loads with bottom strains in single loading. Deflection calculation was developed by mathematically correlating bottom deflections with support loads, and further extended to the concerning region of the non-uniform and opening beam. Validation underwent in loading simulation and tests. The identified deflection deviates from the read and measured within 5.98%. In application, in-transit monitoring reveals that the most unfavorable vertical cargo movement, which is calculated with the identified support deflections and the measured suspension displacement, climbs up to 231.6 mm in synthetic evaluation, when the train runs on a 400-m radius line curve at the speed of 19.6 km/h. The detecting maximum is within but very close to the limit dimension between cargo bottom and rail top, 250 mm. Hence, it is recommended to measure the limit after the transformer is loaded. Research outcome indicates that the proposed approach enables the real-time deflection monitoring and safety evaluation in railway freight transport, which offers scientific evidence for its operation maintenance and structural optimization.

INDEX TERMS Deflection monitoring, load identification, non-uniform beam, opening beam, well-hole freight train, strain measurement.

I. INTRODUCTION

Railway freight transport has always been a strong support for state grid construction programs, especially in delivering over-size cargos including transformers and generator stators [1]. In transport safety, the main concern focuses on the intrusion between the cargo and railway facilities, due to dynamic movement of both the train and cargo [2]. To ascertain safety, dimension check is performed at the two sides and top of loaded cargo according to the loading reinforcement rules [3]. Clearance check of operation facilities is required

The associate editor coordinating the review of this manuscript and approving it for publication was Jesus Felez¹.

along railway lines before transport. However, the risks of collision between cargo bottom and railway bed ballast or station platforms remain unknown. The conflict will damage the cargo, the train body structure [4]–[6] and even result in serious operation accidents including train overturning and derailment, followed with tremendous economic loss and negative social impact [7]–[10].

In railway freight transport, well-hole cars are used to carry transformers. The transformer is loaded on four support bases of two load-carrying beams, which are connected with adjustable bars to fit in transformers of different size. To stop the transformer from relative movement when running on line curves, in acceleration or deceleration, 4 lateral stops are

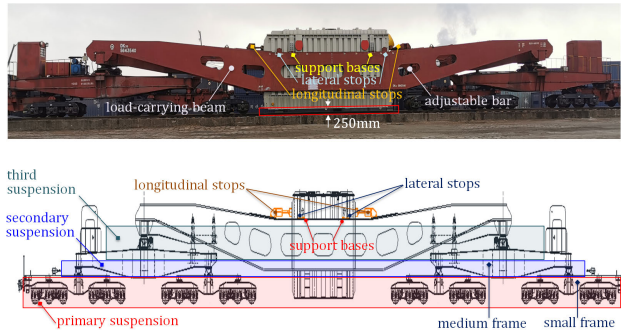


FIGURE 1. Functioning components of DK₃₆-type well-hole freight train.

set beside support bases to stop sliding along its width, and 2 longitudinal stops are designed between two beams to avoid sliding in running direction as Fig. 1.

In running, vertical movement of the loaded transformer consists of two categories, the rigid movement at different suspension and elastic deflection at support bases of load-carrying beams. Vertical rigid movement can be detected by draw-wire displacement sensors at suspensions. But the elastic beam deflection can't be directly measured due to limited space between rail track and transformer (250 mm), not to mention the targeting uncertainty on line curves. Hence, theoretical approach was put forward by formulating the mechanical relation between the elastic deflection and longitudinal strains at support bottoms of D_{26B}-type well-hole cars [11]. The proposed method enables real-time deflection monitoring by multiple strain perception in transit, but unable to work for the DK₃₆-type well-hole car. Because there is no analytical strain-deflection solution of its load-carrying beams, which are non-uniform with opening holes.

In mechanical engineering, structural deflection is a great concern for large girder structures including bridges and wind turbine blades [12]–[14]. To treat with the detection, strain measurement acts as an effective way when it is unlikely to perform a direct deflection measurement [15]. Quasi-static deformation method [16], [17], creates a mechanical correlation of strain-deformation under static load, utilizing the mean curvature [18], least square curve fitting [19]–[22] and conjugate beam method [23], [24]. Displacement-strain transfer function [25]–[29], the other method that uses strain modal theory, acquires the deflection by modal identification with measured strains [30]–[41]. In addition, polynomial fitting between deflection and strains [42], [43] or accelerations [44]–[46], is also employed in dynamic monitoring in bridge deflection and aircraft shape estimation [47]–[51].

Different from the theoretical model of D_{26B}-type well-hole car [8], no analytical solution can be found for the non-uniform opening beam of DK₃₆-type. In this work, a theoretical methodology is proposed for load-carrying beams of DK₃₆-type well-hole freight car. In the second section, mechanical relation of the vertical support loads, strains and deflections at support bottoms, are theoretically modeled via single loading in FEA. The theoretical model is then validated

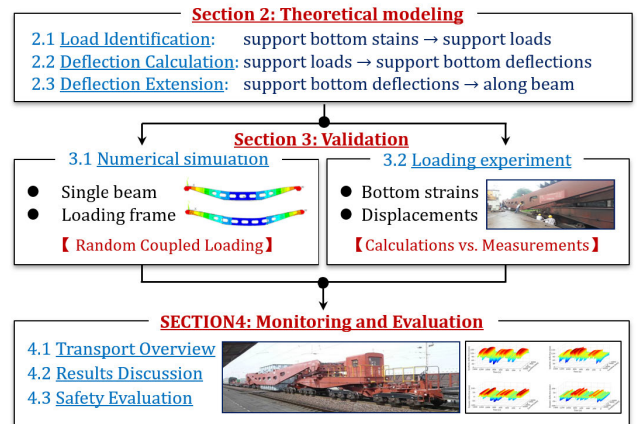


FIGURE 2. Paper framework and technical route.

by simulation of random coupled loading, as well as on-site loading test in third section. In the fourth section, the proposed method is applied in real-vehicle test. The maximum deflection and safety evaluation are discussed. The framework of this paper is shown as Fig. 2.

II. THEORETICAL MODELING

Load-carrying beam of DK₃₆-type well-hole car, with non-uniform sections and opening holes, is simply supported on the lateral supporting beams at the two ends. Vertical support loads at the two support bases, are defined by F_1 and F_2 , respectively. Longitudinal strains and vertical deflections at support bottoms, are denoted by ϵ_1 and ϵ_2 , ω_1 and ω_2 , respectively. In transformer loading, geometrical dimensions and external forces of the beam model is illustrated in Fig. 3. The material is HG70 high-strength steel for the beam, and Q345 low-alloy steel for linking bars. The elastic modulus (E) is 210000 MPa, the Poisson ratio (μ) is 0.3 and the density (ρ) is 7680 kg/m³. Geometry dimension of the load-carrying beam is listed in Table 1.

In theoretical modeling, FEA method is adopted to acquire the mechanical relation between longitudinal strains at support bottoms (ϵ_1 and ϵ_2) and vertical loads at support bases (F_1 and F_2). In a same way, correlation between support bottom deflections (ω_1 and ω_2) and identified support loads (F_1 and F_2) is given by single loading simulation. As a result, deflection calculation is modeled where the measured strains at support bottoms (ϵ_1 and ϵ_2) are the input parameters, vertical deflections (ω_1 and ω_2) are the output. Output deflections are extended to acquire deflections at all location of load-carrying beam in concerning safety-relevant region.

A. LOAD IDENTIFICATION

The loading frame of DK₃₆-type well-hole car is subjected to vertical forces from transformer through support bases, lateral curve-running centrifugal force from lateral stops, longitudinal forces from acceleration or deceleration through longitudinal stops. Lateral and longitudinal forces can be directly measured by pressure sensors installed between

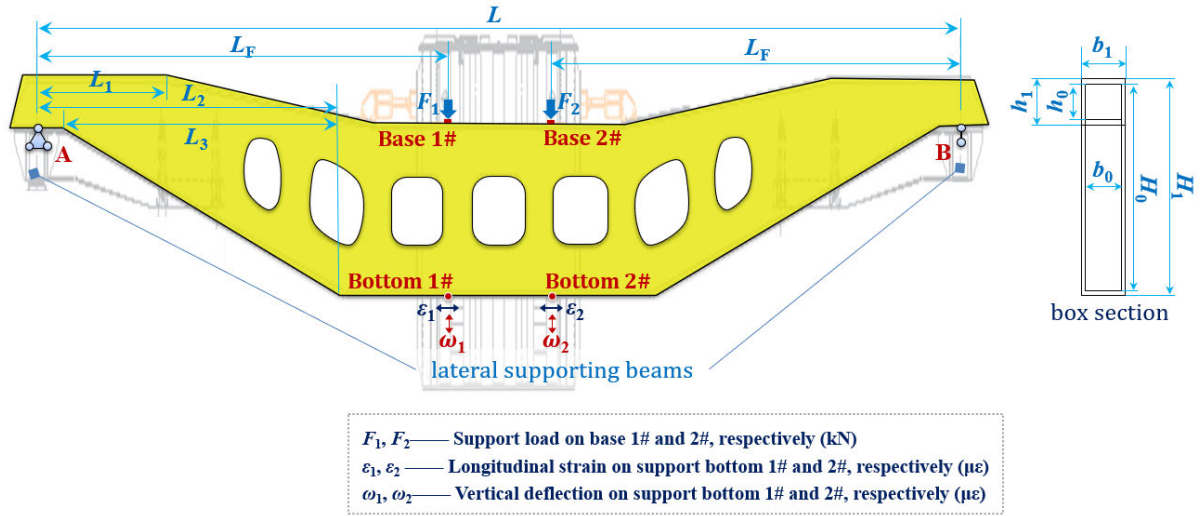


FIGURE 3. Mechanical model of non-uniform opening load-carrying beam.

TABLE 1. Geometric dimensions.

Dimensions	L	L_1	L_2	L_3	H_1	H_0	h_1	h_0	L_F	b_1	b_0
Value (Unit: mm)	36000	1000	12000	11000	12470	12350	460	340	14675	214	178

transformer and stop structures. But for the vertical, it's unlikely to perform a direct measurement because the transformer base and support base are welded together. Hence, the vertical forces are identified by detecting the strains, which locates at the support bottom. The linear correlation between support bottom strains and support loads in the elastic mechanical stage, is created by single loading simulation, as in Fig. 4. In load identification, further step is taken to fit the model in different support locations due to different transformer size.

In single support loading at base 1#, the vertical load is denoted by F_1 , strains at two support bottoms are denoted by ϵ_{1_F1} and ϵ_{2_F1} , respectively. In linear elastic stage, bottom strains are formulated as

$$\epsilon_{1_F1} = a_{1_F1} \cdot F_1 \tag{1a}$$

$$\epsilon_{2_F1} = a_{2_F1} \cdot F_1 \tag{1b}$$

where a_{1_F1} and a_{2_F1} are the fitting coefficients between load at support base 1# and strain at two support bottoms, respectively.

In support loading at base 2#, the vertical load is denoted by F_2 . Strains at two support bottoms, which are denoted by ϵ_{1_F2} and ϵ_{2_F2} , respectively, are formulated as

$$\epsilon_{1_F2} = a_{1_F2} \cdot F_2 \tag{2a}$$

$$\epsilon_{2_F2} = a_{2_F2} \cdot F_2 \tag{2b}$$

where a_{1_F2} and a_{2_F2} are the fitting coefficients between load at support base 2# and strain at two support bottoms, respectively.

The detected strain at each support bottom, respectively denoted by ϵ_1 and ϵ_2 , is composed of strains induced by the two support loads, respectively. Thus,

$$\epsilon_1 = \epsilon_{1_F1} + \epsilon_{1_F2} = a_{1_F1} \cdot F_1 + a_{1_F2} \cdot F_2 \tag{3a}$$

$$\epsilon_2 = \epsilon_{2_F1} + \epsilon_{2_F2} = a_{2_F1} \cdot F_1 + a_{2_F2} \cdot F_2 \tag{3b}$$

Accordingly, the support forces are identified by

$$F_1 = \frac{a_{2_F2} \cdot \epsilon_1 - a_{1_F2} \cdot \epsilon_2}{a_{1_F1} \cdot a_{2_F2} - a_{2_F1} \cdot a_{1_F2}} \tag{4a}$$

$$F_2 = \frac{a_{1_F1} \cdot \epsilon_2 - a_{2_F1} \cdot \epsilon_1}{a_{1_F1} \cdot a_{2_F2} - a_{2_F1} \cdot a_{1_F2}} \tag{4b}$$

In transformer loading of DK₃₆-type well-hole car, the geometry dimensions remain constant except the support location (L_F) because of different transformer size. To make a general solution, mechanical relation between strain-force coefficients and support location (L_F) is mathematically modeled with simulation results in 9 different support locations. Locations are determined by the range of support base distance when loading transformers with different weight and size.

Considering the geometry and loading symmetry, we have

$$a_{1_F1} = a_{2_F2} = f_{1_F1}(L_F) = f_{2_F2}(L_F) \tag{5a}$$

$$a_{2_F1} = a_{1_F2} = f_{2_F1}(L_F) = f_{1_F2}(L_F) \tag{5b}$$

The support load identification can therefore be simplified as in (6).

$$F_1 = \frac{f_{1_F1}(L_F) \cdot \epsilon_1}{f_{1_F1}^2(L_F) - f_{2_F1}^2(L_F)} - \frac{f_{2_F1}(L_F) \cdot \epsilon_2}{f_{1_F1}(L_F) - f_{2_F1}^2(L_F)} \tag{6a}$$

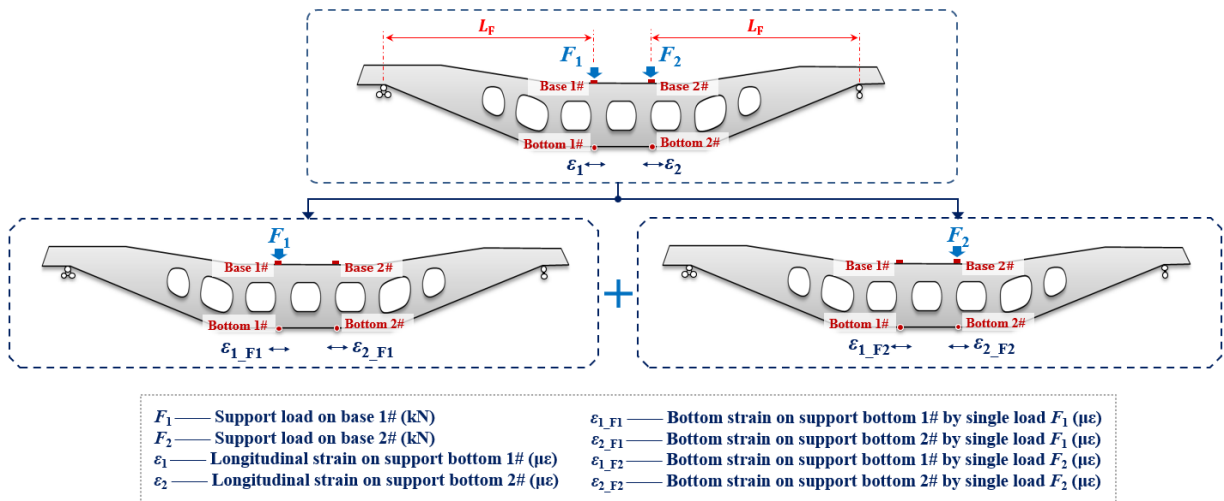


FIGURE 4. Strain calculation consisting of individual support load simulation.

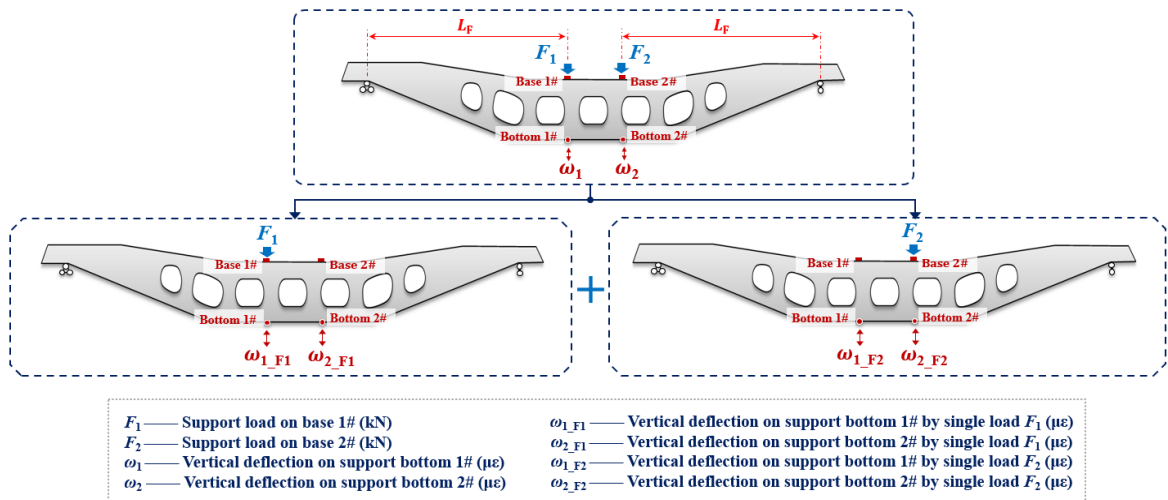


FIGURE 5. Deflection calculation consisting of individual support load simulation.

$$F_1 = \frac{f_{2_F1}(L_F) \cdot \varepsilon_1}{f_{2_F1}^2(L_F) - f_{1_F1}^2(L_F)} - \frac{f_{1_F1}(L_F) \cdot \varepsilon_2}{f_{2_F1}^2(L_F) - f_{1_F1}^2(L_F)} \quad (6b)$$

B. DEFLECTION CALCULATION

In deflection calculation, the identified support load serves as medium variable to relate the deflection and the measurable strain. Likewise, the deflection is decoupled into deflections induced by each support load, as in Fig. 5, and transferred into the formulation based on the strain acquired in the previous section.

In single loading at base 1#, support bottom deflections are denoted by ω_{1_F1} and ω_{2_F1} , respectively. Mechanical relations are given with different support locations as

$$\omega_{1_F1} = g_{1_F1}(L_F) \cdot F_1 \quad (7a)$$

$$\omega_{2_F1} = g_{2_F1}(L_F) \cdot F_1 \quad (7b)$$

where $g_{1_F1}(L_F)$ and $g_{2_F1}(L_F)$ are the coefficients between support load F_1 and deflection at two supports, respectively.

In single loading at base 2#, vertical deflections at two support bottoms are denoted by ω_{1_F2} and ω_{2_F2} respectively. Formulations are given as

$$\omega_{1_F2} = g_{1_F2}(L_F) \cdot F_2 \quad (8a)$$

$$\omega_{2_F2} = g_{2_F2}(L_F) \cdot F_2 \quad (8b)$$

where $g_{1_F2}(L_F)$ and $g_{2_F2}(L_F)$ are the coefficients between support load F_2 and deflections at two supports, respectively.

The practical deflection at each support bottom is composed of deflections induced by the two support loads, respectively.

$$\omega_1 = g_{1_F1}(L_F) \cdot F_1 + g_{1_F2}(L_F) \cdot F_2 \quad (9a)$$

$$\omega_2 = g_{2_F1}(L_F) \cdot F_1 + g_{2_F2}(L_F) \cdot F_2 \quad (9b)$$

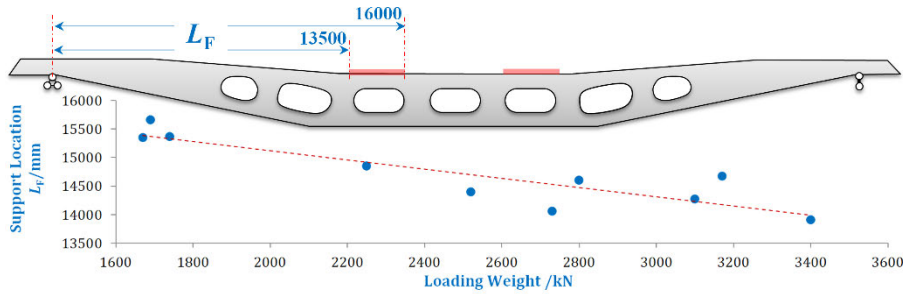


FIGURE 6. Deflection calculation consisting of individual support load simulation.

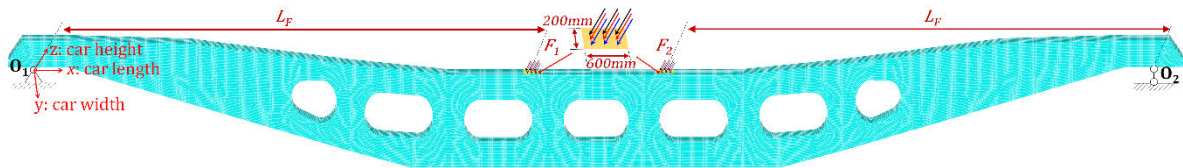


FIGURE 7. Boundary and loading conditions of load-carrying beam model.

Because of the geometry and loading symmetry, we have: $g_{1_F1}(L_F) = g_{2_F2}(L_F)$, $g_{1_F2}(L_F) = g_{2_F1}(L_F)$. Therefore, the support bottom deflections are calculated by

$$\omega_1 = C_1(L_F) \cdot \varepsilon_1 - C_2(L_F) \cdot \varepsilon_2 \quad (10a)$$

$$\omega_2 = -C_2(L_F) \cdot \varepsilon_1 + C_1(L_F) \cdot \varepsilon_2 \quad (10b)$$

where

$$C_1(L_F) = \frac{g_{1_F1}(L_F) \cdot f_{1_F1}(L_F) - g_{2_F1}(L_F) \cdot f_{2_F1}(L_F)}{f_{1_F1}^2(L_F) - f_{2_F1}^2(L_F)} \quad (11a)$$

$$C_2(L_F) = \frac{g_{1_F1}(L_F) \cdot f_{2_F1}(L_F) - g_{2_F1}(L_F) \cdot f_{1_F1}(L_F)}{f_{1_F1}^2(L_F) - f_{2_F1}^2(L_F)} \quad (11b)$$

To calculate the mathematic function of strain-load ($f_{1_F1}(L_F)$, $f_{2_F1}(L_F)$) and load-deflection ($g_{1_F1}(L_F)$, $g_{2_F1}(L_F)$), support location L_F is defined in the range of 13500~16000 mm according to historical transport of transformers, the weight of which varies from 1670 kN to 3400 kN, as in Fig. 6.

To better fit the correlation between support location and strain-load coefficient, as well as load-deflection coefficient, the support location range is divided into 8 segments, 9 locations. At each location, vertical support load is defined into 4 step loads, the maximum of which is the mean of the total 4 support loads at the transporting limit of DK₃₆-type, 3600 kN.

In FEA, Hypermesh was used to create the finite element mesh of the load-carrying beam, and the simulation was performed in ANSYS. The thickness of the beam is only 18 mm comparing with its length (36m) and height (12.47m), the thin-walled structure is therefore meshed with shell elements. The minimum size of beam boundaries in irregular

shapes, is smaller than 60mm. In order to ensure adequate efficiency and accuracy in FEA, the mesh size was set to 20 mm. The load-carrying beam is modeled and meshed with 145060 nodes and 147613 shell elements, as in Fig. 7.

Translation constraints are defined at both ends of the beam model. Longitudinal translation is released at one end to let go the movement in longitudinal deformation. Concentrating forces are defined at two supporting area of 600 mm×220 mm, describing the actual area of support bases, as in Fig.7.

The vertical displacement and longitudinal strain at the bottom line of load-carrying beam, which ranges from -6000 mm to 6000 mm centering its symmetry axis, is responsible for large deflection. The bottom deflection in the concerning region under single support loading of 900 kN, which is 1/4 of the loading capacity of well-hole car (3600 kN), is given in Fig. 8(a) with different support locations. It is revealed that as the support location approaches the middle, there is an increase on the maximum deflection (52.95~57.17 mm) and deflection at support bottoms (51.92~56.84 mm at support 1#, 44.68~54.54 mm at support 2#). Despite the holes in the beam, vertical deflection monotonically rises from two sides to the peak, revealing a different rule as longitudinal strains depicted in Fig. 8(b). The inflection point of longitudinal strain arises at hole boundaries where its semicircle and rectangle meet, as the red bar describes in Fig. 8(b). In addition, minor strain changes can be observed at the middle axis of the hole and between holes, as the dash dot line suggests. To find mechanical relation between support forces, bottom strains and support locations, mathematical formulation between strain-load coefficient and support location is given in priority.

Reading the longitudinal strains and vertical deflections at support bottoms, simulation results and fitting coefficients of

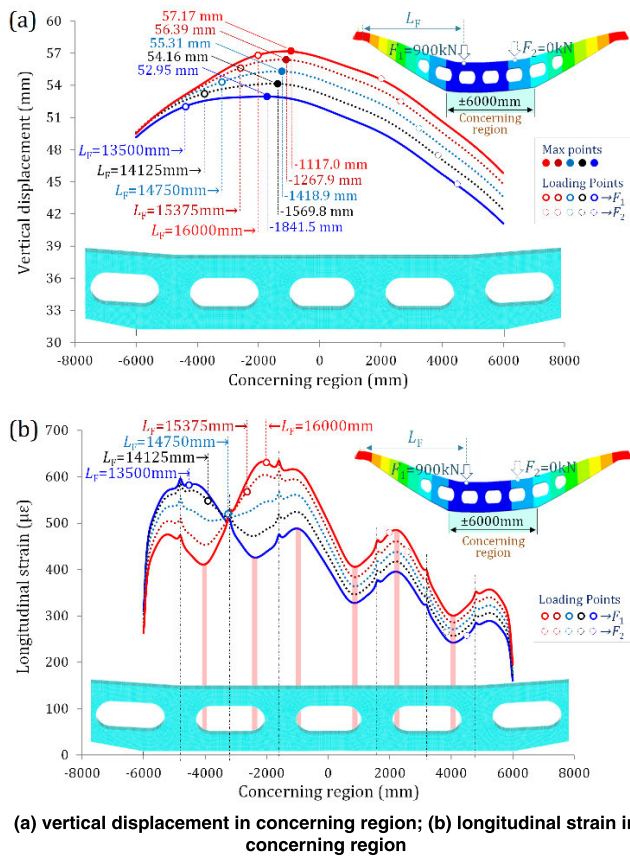


FIGURE 8. Deflection and strain under single loading of 900 kN in different load locations.

strain-load, deflection-load are given in Fig. 9 under single loading with 4 load magnitudes and 9 support locations, in an attempt to make a more precise model.

Linear correlation between strain-load and displacement-load is observed in simulation, by fitting the data of strain and displacement in different load magnitudes, but at the same support location. However, strain-load coefficient and support location L_F follows a 4th-order polynomial correlation where the fitting degree can reach 0.99. Different from strain-load coefficient, there is a linear correlation between deflection-load coefficient and support location. The analytical expression of strain-load coefficient and deflection-load with respect to support location, are given by (12).

$$f_{1_F1}(L_F) = -5.8242 \times 10^{-14} L_F^4 + 3.436696 \times 10^{-9} L_F^3 - 7.588679 \times 10^{-5} L_F^2 + 0.743198 L_F - 2723.2062 \quad (12a)$$

$$f_{2_F1}(L_F) = -6.874066 \times 10^{-15} L_F^4 + 3.638048 \times 10^{-10} L_F^3 - 7.093347 \times 10^{-6} L_F^2 + 6.020383 \times 10^{-2} L_F - 186.476727 \quad (12b)$$

$$g_{1_F1}(L_F) = 2.1949 \times 10^{-6} L_F + 0.0280 \quad (12c)$$

$$g_{2_F1}(L_F) = 4.4729 \times 10^{-6} L_F - 0.0106 \quad (12d)$$

Based on theoretical modeling and FE simulation, support load identification and bottom deflection calculation are formulated by (6), (10), (11) and (12). Only the deflection at two support bottoms is concerned because it accounts for the vertical beam deformation that brings about the vertical movement of the transformer.

C. DEFLECTION EXTENSION

In the previous part, support loads and deflections are formulated with pre-calculated constants. Support load and deflection calculation via strain measurement, is a simple arithmetic operation. If there is a need to observe deflections along the bottom beam in concerning region, the polynomial fitting method is employed between deflection curve and identified support loads.

At the 9 predefined support locations, the deflection curve can be formulated by fitting each under the single support loading of 900 kN, whereas the fitting constants can be linearly formed with other load magnitudes at the same support location. In this way, the fitting equations of vertical displacement in the concerning region are given at support locations ranging from 13500 mm to 16000 mm, under load magnitude of 900 kN, as seen in Fig. 10(a). Also, the correlation between fitting constants A_i, B_i, C_i , and support locations (as in Table 2), based on which the deflection curve can be modeled under 900-kN load magnitude, are then given as in (13).

$$\omega_{F1}(x) = A \cdot x^2 + B \cdot x + C = [A(L_F) \cdot x^2 + B(L_F) \cdot x + C(L_F)] \cdot F_1 / 900 \quad (13a)$$

$$A(L_F) = C_{A1} \cdot L_F + C_{A2} \quad (13b)$$

$$B(L_F) = C_{B1} \cdot L_F + C_{B2} \quad (13c)$$

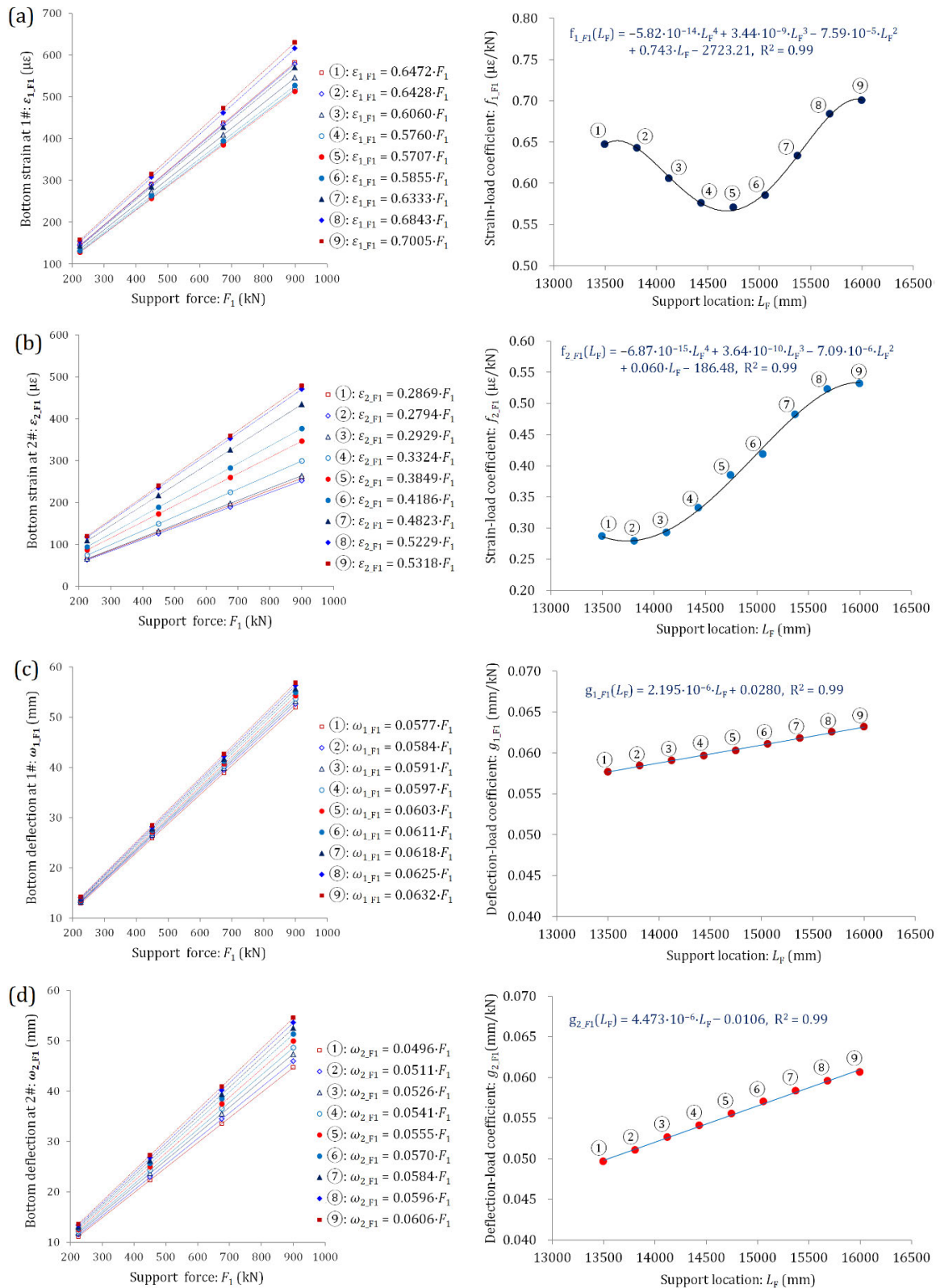
$$C(L_F) = C_{C1} \cdot L_F + C_{C2} \quad (13d)$$

where $\omega_{F1}(x)$ is the deflection expression in single support loading. A, B and C are the fitting constants in different support locations under load magnitude of 900 kN. For constants A, B , and C , the fitting coefficients with respect to support location L_F are denoted by $C_{A1} (2.928 \cdot 10^{-11} \text{ mm}^{-2})$, $C_{A2} (-6.5332 \cdot 10^{-7} \text{ mm}^{-1})$, $C_{B1} (-1.6165 \cdot 10^{-7} \text{ mm}^{-1})$, $C_{B2} (-1.7963 \cdot 10^{-3})$, $C_{C1} (-1.8376 \cdot 10^{-3})$ and $C_{C2} (82.10 \text{ mm})$, according to the fitting results in Fig. 10(b).

The deflection calculation can be extended with respect to the load magnitude F_1 and support location L_F , by blending the four equations from (13) with linear conversion from magnitude of 900 kN to others. The ultimate formulation of vertical deflection under single loading is given in (14) as follows:

$$\omega_{F1}(x, F_1, L_F) = \frac{C_{A1} \cdot L_F + C_{A2}}{900} \cdot F_1 \cdot x^2 + \frac{C_{B1} \cdot L_F + C_{B2}}{900} \cdot F_1 \cdot x + \frac{C_{C1} \cdot L_F + C_{C2}}{900} \cdot F_1 \quad (14)$$

Taking account into the geometry and loading symmetry, the beam deflection curve $\omega_{F2}(x)$ can be re-formulated in single support loading of F_2 , by letting $t = -x$ and $F_1 = F_2$,



(a) strain-load coefficient at support 1#; (b) strain-load coefficient at support 2#; (c) deflection-load coefficient at support 1#; (d) deflection-load coefficient at support 2#

FIGURE 9. Fitting curve of strain-load and deflection-load coefficient vs. support location under single loading at support 1#.

TABLE 2. Fitting coefficients vs. support locations.

Support Locations L_F (mm)	Fitting Coefficients		
	A_i (mm ⁻¹)	B_i (l)	C_i (mm)
16000.0	$-1.86 \cdot 10^{-7}$	$-7.76 \cdot 10^{-4}$	52.01
15687.5	$-1.93 \cdot 10^{-7}$	$-7.41 \cdot 10^{-4}$	52.64
15375.0	$-2.02 \cdot 10^{-7}$	$-6.95 \cdot 10^{-4}$	53.31
15062.5	$-2.11 \cdot 10^{-7}$	$-6.48 \cdot 10^{-4}$	53.94
14750.0	$-2.21 \cdot 10^{-7}$	$-5.96 \cdot 10^{-4}$	54.55
14437.5	$-2.33 \cdot 10^{-7}$	$-5.38 \cdot 10^{-4}$	55.19
14125.0	$-2.42 \cdot 10^{-7}$	$-4.85 \cdot 10^{-4}$	55.72
13812.5	$-2.50 \cdot 10^{-7}$	$-4.30 \cdot 10^{-4}$	56.22
13500.0	$-2.55 \cdot 10^{-7}$	$-3.84 \cdot 10^{-4}$	56.59

as in (15).

$$\omega_{F2}(x, F_2, L_F) = \frac{C_{A1} \cdot L_F + C_{A2}}{900} \cdot F_2 \cdot x^2 + \frac{C_{B1} \cdot L_F + C_{B2}}{900} \cdot F_2 \cdot x + \frac{C_{C1} \cdot L_F + C_{C2}}{900} \cdot F_2 \quad (15)$$

The resultant deflection is the summation of two individual deflection curve induced by each single loading, as in (16).

$$\omega(x) = \left(\frac{C_{A1} \cdot L_F + C_{A2}}{900} \cdot x^2 + \frac{C_{C1} \cdot L_F + C_{C2}}{900} \right) \cdot (F_1 + F_2) + \frac{C_{B1} \cdot L_F + C_{B2}}{900} \cdot (F_1 - F_2) \cdot x \quad (16)$$

The constant of quadratic term (A_i) remains negative, a maximum of deflection as well as its location can therefore be found as follows:

where ω_{MAX} is the maximum deflection and x_{MAX} is its location in concerning region.

Hence, (16) offers a theoretical model for calculating the deflection curve in identified support loads, and (17) gives a calculation of the maximum deflection and its location.

III. VALIDATION

Validation goes in numerical simulation and on-site loading experiment. In simulation, support location, load magnitude at two support bases are randomly generated as load cases in the range of practical scenarios. 10 load cases of coupled support loading are given to verify the proposed model. The difference is compared between the identifications and given loads as well as read deflections in simulation.

In loading experiment, strains and deflections are measured at support bottoms before and after transformer loading. The measured strains are substituted into the proposed model to identify the support forces and static deflections, which are compared with practical forces and measured deflections.

A. NUMERICAL SIMULATION

The FE model and boundary condition of single beam in simulation validation remain the same as in theoretical modeling. To compare the results of each beam on the full assembled loading frame, simulation validation is also conducted on the loading frame. The frame is modeled and meshed with 418475 nodes and 425799 elements, including 424399 shell elements for load-carrying beams and 1400 beam elements of linking bars, as in Fig. 11. Likewise, in single beam, the mesh size of loading frame was set to 20mm. The two marked areas at the bottom of lateral beam on one end, are defined with full constraints except the rotation about car width direction. Symmetric areas on the other end are defined with only vertical constraint. Vertical loads are defined the same way as in single load-carrying beam.

To cover possible loading scenarios, 10 load cases were generated by random method concerning the range of two support forces and support locations. Since the theoretical modeling is carried out on single support loading, only coupled loading at two support bases is taken into account here. Single beam and loading frame model are involved in validation, the two support forces and loading location are the same on the two beams of loading frame in accord with practical circumstance. The support force varies in the range of 0~900 kN at each base. The loading location ranges from 13500 mm to 16000 mm. Validation load cases are listed in Table 3.

For each load case, longitudinal strains at two support bottoms are read and substituted into the load identification and deflection calculation model. The identified support load magnitude and deflection (denoted as 'ID') are compared with the given loads and read deflections (denoted as 'GV') in Table 4. Relative deviation is calculated by $|'ID' - 'GV'|/'GV' \times 100\%$ and plotted in a 3D bar as Fig.12.

Comparison indicates that the deviation ($|'ID' - 'GV'|$) between identified and given loads, varies within 35.5 kN for load magnitudes, and 2.4 mm for support deflections. The relative deviation ranges within 5.98% and 3.28% for load magnitudes and support deflections, respectively. Relative deviation goes no more than 6%, which suggests good agreement of the proposed method with simulation. It is also seen that the relative deviation is smaller in single beam validation than that in loading frame. In load validation, the maximum relative deviation is 2.12% in single beam simulation and 5.98% in loading frame simulation. In deflection validation, the maximum relative deviation is 0.64% in single beam and 3.27% in loading frame. To explain the difference, the mechanical response of the lateral supporting beam, which support the two load-carrying beams at two ends, are taken into account. The bending effect of lateral beams give rise to a higher deviation, but fortunately no greater than 6%.

B. LOADING EXPERIMENT

In transformer loading, two load-carrying beams are adjusted in a distance of 3560 mm, and the lateral distance between

TABLE 3. Load cases in simulation validation by random method.

Parameter / Function	F_1 (0~900kN) 900[1-rand()]	F_2 (0~900kN) 900[1-rand()]	L_F (13500~16000mm) 16000-2500·rand()
Load case 1#	760	582	14310
Load case 2#	495	709	13860
Load case 3#	141	752	15860
Load case 4#	277	387	15470
Load case 5#	403	495	13890
Load case 6#	92	780	13710
Load case 7#	815	506	15890
Load case 8#	132	205	14548
Load case 9#	613	659	15680
Load case 10#	625	829	14070

NOTE: ‘rand()’ is the random function that varies in the range of 0.0-1.0. Support loads and location are the same on two beams of loading frame model.

side beam and transformer boundary is 60 mm. The loaded transformer weighs 3170 kN (denoted as F_G), the support distance of which is 6650 mm in its length. The geometric center of the loading frame deviates 200 mm from transformer gravity center in longitudinal, but coincides laterally. Loading dimensions of both frame and the cargo is depicted in Fig. 13.

During the loading test, strains at support bottoms are measured by strain gauges and read from data acquisition system (DAQ). Deflections are measured with steel tape and plumb line, in terms of the displacement at assembly ends, support bottoms and middle bottom of load-carrying beam, as in Fig. 14. Displacement measurement is carried out in a way that the distance is characterized by the length of plumb line in strict vertical direction to rail head, and measured by steel tape afterwards. Loading deflections are calculated by measured displacements as in (18).

$$D_{S1} = (D_{S1_UL} - D_{S1_LD}) - \left[\frac{(L-L_F) \cdot (D_{1_UL} - D_{1_LD}) + L_F \cdot (D_{2_UL} - D_{2_LD})}{L} \right] \quad (18a)$$

$$D_{S2} = (D_{S2_UL} - D_{S2_LD}) - \left[\frac{(L-L_F) \cdot (D_{2_UL} - D_{2_LD}) + L_F \cdot (D_{1_UL} - D_{1_LD})}{L} \right] \quad (18b)$$

$$D_M = (D_{M_UL} - D_{M_LD})$$

$$\frac{(D_{1_UL} - D_{1_LD} + D_{2_UL} - D_{2_LD})}{2} \quad (18c)$$

where D_{S1} and D_{S2} are the static deflection at two support bottoms. D_M is the deflection at the middle bottom. D_{1_UL} and D_{2_UL} are the distance of lateral support beams from railhead before loading. D_{1_LD} and D_{2_LD} represent the distance of that after loading. D_{S1_UL} and D_{S2_UL} are the distance of the two support bottoms from railhead before loading. D_{S1_LD} and D_{S2_LD} are the distance of that after loading. D_{M_UL} and D_{M_LD} are the distance of the middle bottom from railhead before and after loading, respectively.

The support forces are theoretically calculated due to the difficulty in performing direct measurement, because the support bases are welded with the cargo bases. Identified support forces are then compared with theoretical calculations at support bases, which are given in (19) using the force and moment equilibrium as follows:

$$F_{1_L} = (L_W + 2\Delta_W) \cdot (L_S + 2\Delta_L) \cdot F_G / (4L_S \cdot L_W) \quad (19a)$$

$$F_{2_L} = (L_W + 2\Delta_W) \cdot (L_S - 2\Delta_L) \cdot F_G / (4L_S \cdot L_W) \quad (19b)$$

$$F_{1_R} = (L_W - 2\Delta_W) \cdot (L_S + 2\Delta_L) \cdot F_G / (4L_S \cdot L_W) \quad (19c)$$

$$F_{2_R} = (L_W - 2\Delta_W) \cdot (L_S - 2\Delta_L) \cdot F_G / (4L_S \cdot L_W) \quad (19d)$$

where F_{1_L} and F_{2_L} are the theoretical support forces on the left beam, F_{1_R} and F_{2_R} are the theoretical support forces on the right beam. The direction of two beams is distinguished when the train is moving forward in top view. L_S is the longitudinal distance between support bases on each beam, here $L_S = 6650\text{mm}$. L_W is the lateral distance of support base

$$\omega_{MAX} = \frac{4(C_{A1} \cdot L_F + C_{A2}) \cdot (C_{C1} \cdot L_F + C_{C2}) \cdot (F_1 + F_2)^2 - (C_{B1} \cdot L_F + C_{B2})^2 \cdot (F_1 - F_2)^2}{3600(C_{A1} \cdot L_F + C_{A2}) \cdot (F_1 + F_2)} \quad (17a)$$

$$x_{MAX} = \frac{(C_{B1} \cdot L_F + C_{B2}) \cdot (F_2 - F_1)}{2(C_{A1} \cdot L_F + C_{A2}) \cdot (F_1 + F_2)} \quad (17b)$$

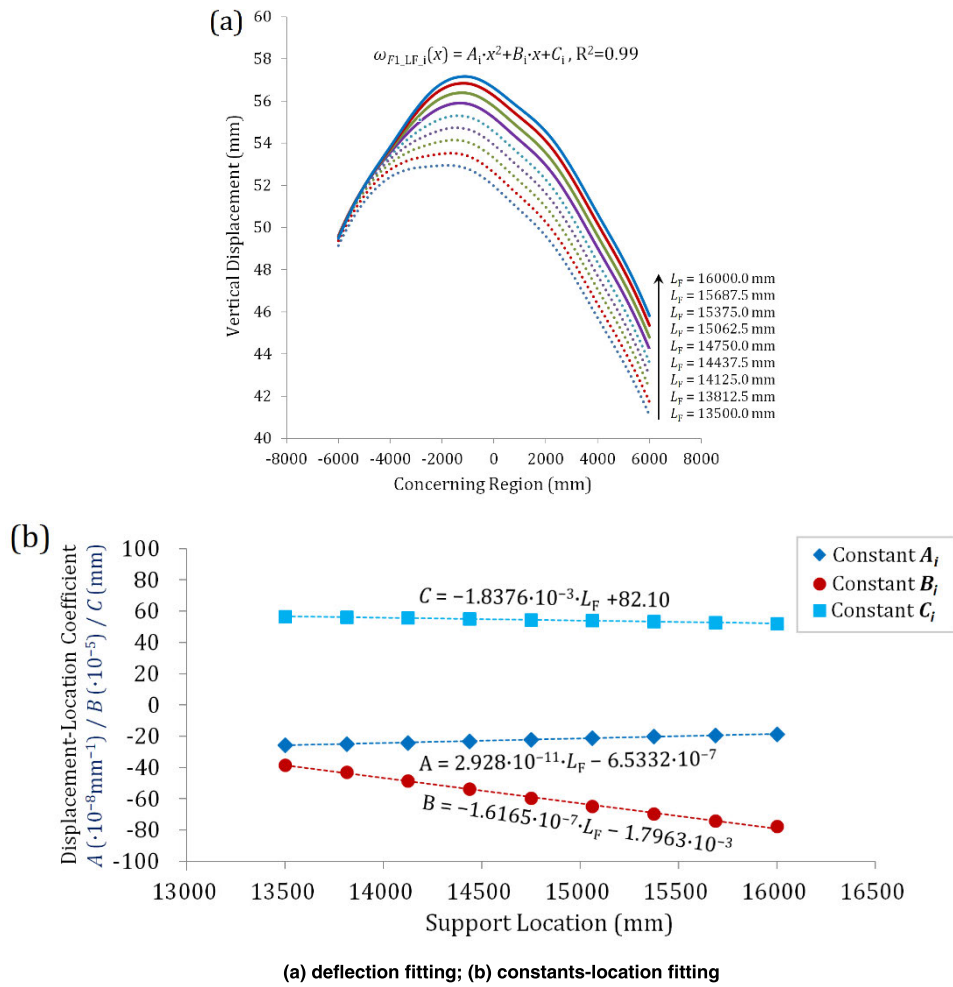


FIGURE 10. Deflection curve formulation under single loading of 900 kN at support 1#.

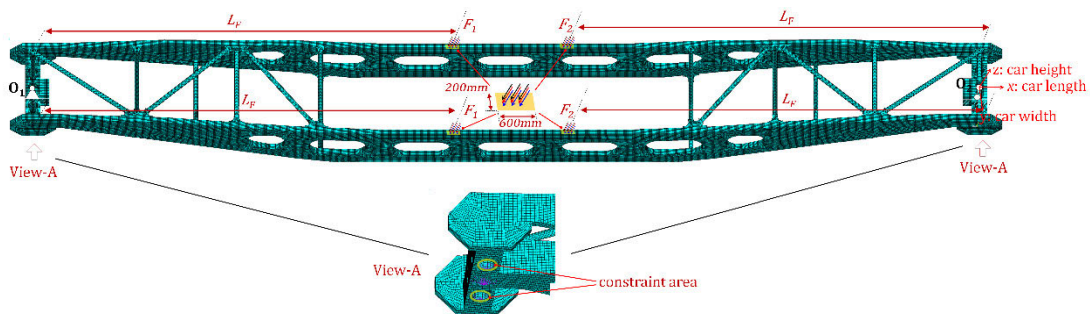


FIGURE 11. Boundary and loading conditions of loading frame FEA model.

between two beams, and $L_W = 3560\text{mm}$. Δ_L and Δ_W are the deviation of transformer gravity center from the support base center line in car length and width direction, respectively, here $\Delta_L = 200\text{ mm}$ and $\Delta_W = 0\text{ mm}$. F_G is the gravity load of transformer, here $F_G = 3170\text{ kN}$. Hence, theoretical vertical forces are $F_{1_L} = F_{1_R} = 864\text{ kN}$, $F_{2_L} = F_{2_R} = 721\text{ kN}$.

Strain measurement output is set to zero before loading. Strains at 4 support bottoms of two beams are read from

DAQ system after loading, $\epsilon_{1_L} = 735\ \mu\epsilon$ and $\epsilon_{2_L} = 708\ \mu\epsilon$ at two support bottoms on the left beam, $\epsilon_{1_R} = 744\ \mu\epsilon$ and $\epsilon_{2_R} = 726\ \mu\epsilon$ at two support bottoms on the right beam. Measured strains are substituted into the model, in an attempt to acquire the support forces and vertical deflections by the proposed method. Comparison is made between identified and given results in loading experiment as Table 5.

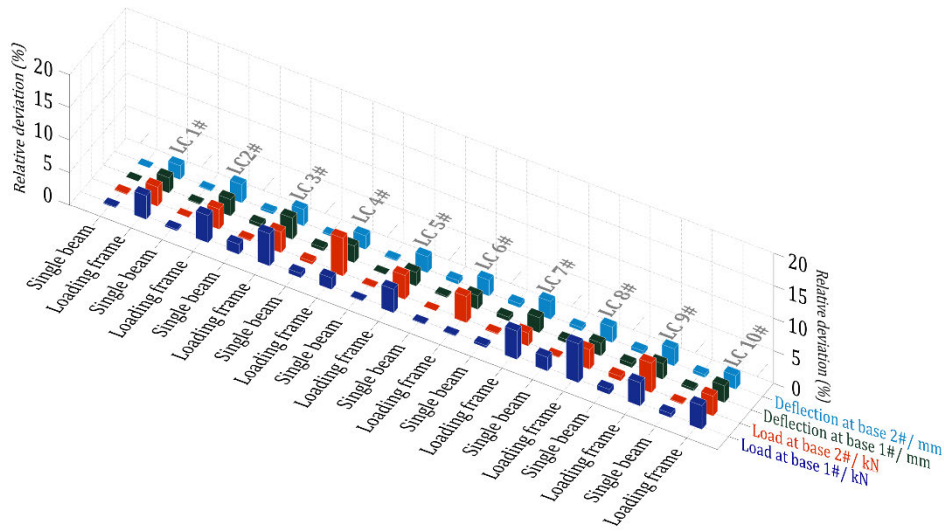


FIGURE 12. Relative support load and deflection deviation in random simulation validation. NOTE: ‘LC’ is short for ‘Load Case’.

TABLE 4. Comparison between identified and given results in validation simulation.

Load case	Bottom Strain / $\mu\epsilon$		Load Magnitude /kN				Support deflection /mm				
	ϵ_1	ϵ_2	F_1		F_2		ω_1		ω_2		
			ID	GV	ID	GV	ID	GV	ID	GV	
1#	Single beam	628.6	580.3	761.1	760	582.9	582	76.3	76.3	75.3	75.3
	Loading frame	649.5	598.3	787.9	760	599.2	582	78.8	80.7	77.7	79.4
2#	Single beam	513.8	590.5	493.8	495	709.3	709	65.3	65.4	66.8	66.9
	Loading frame	534.0	610.6	515.7	495	731.2	709	67.7	69.5	69.2	71.2
3#	Single beam	499.7	601.4	143.2	141	753.3	752	54.4	54.1	56.0	55.8
	Loading frame	515.0	619.8	148.0	141	776.0	752	56.1	58.0	57.7	59.2
4#	Single beam	372.8	389.7	278.9	277	388.7	387	40.1	39.9	40.4	40.3
	Loading frame	385.1	404.7	281.9	277	409.6	387	41.5	42.6	41.9	42.8
5#	Single beam	394.6	427.0	402.6	403	494.6	495	49.0	49.0	49.7	49.6
	Loading frame	409.5	443.1	417.6	403	513.3	495	50.9	52.0	51.5	52.8
6#	Single beam	277.8	531.4	92.1	92	780.3	780	44.9	45.0	50.0	50.3
	Loading frame	286.5	551.6	92.1	92	811.5	780	46.5	47.5	51.8	53.1
7#	Single beam	841.3	789.3	817.9	815	506.9	506	82.1	81.6	81.3	80.8
	Loading frame	869.0	813.1	850.5	815	516.2	506	84.7	86.7	83.9	86.3
8#	Single beam	147.3	162.9	134.8	132	204.8	205	19.2	19.1	19.6	19.5
	Loading frame	152.4	168.3	139.9	132	211.2	205	19.9	20.3	20.3	20.8
9#	Single beam	764.0	771.5	617.8	613	663.7	659	78.1	77.6	78.2	77.8
	Loading frame	788.7	797.5	635.0	613	688.9	659	80.6	82.6	80.8	83.0
10#	Single beam	622.0	688.4	621.0	625	827.7	829	79.9	80.2	81.2	81.6
	Loading frame	646.2	712.5	647.9	625	854.3	829	82.9	85.1	84.2	86.0

NOTE: ‘ID’ represents ‘Identified’. ‘GV’ represents ‘Given’, including the predefined load magnitude and the displacement read at support bottoms in simulation.

Result listed above reveals that the strains, support forces and deflections at support base 1#, measured or identified, are greater than that on support base 2#. Identified support forces deviate from theoretical calculations within 2.41%

and 3.38% on the left and right beam, respectively. Identified deflections deviate from measurement within 2.39% and 1.83% on the left and right beam, respectively. Results suggest good agreement between the proposed method and on-

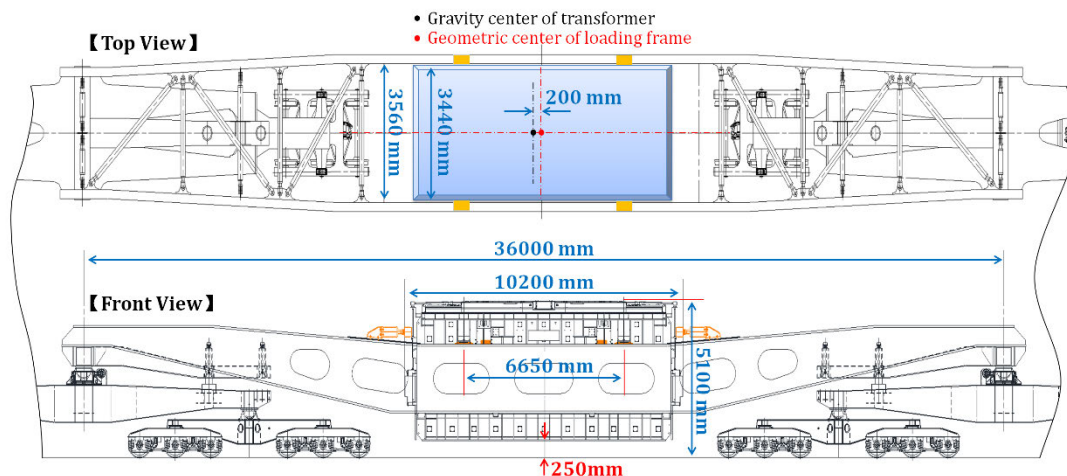


FIGURE 13. On-site loading dimension of transformer and the frame structure.



FIGURE 14. On-site measurement of static deflection and strains.

TABLE 5. Comparison between identified and given results in loading experiment.

Mechanical parameters	Left beam					Right beam				
	Force (kN)		Deflection (mm)			Force (kN)		Deflection (mm)		
	SPT 1# (F_{1L})	SPT 2# (F_{2L})	SPT 1# (D_{S1})	SPT 2# (D_{S2})	Middle (D_M)	SPT 1# (F_{1R})	SPT 2# (F_{2R})	SPT 1# (D_{S1})	SPT 2# (D_{S2})	Middle (D_M)
Identified	843.1	708.4	89.8	89.1	95.3	835.2	745.4	91.3	90.9	96.9
Theoretical /Measured	864.0	721.0	92.0	91.0	97.0	864.0	721.0	93.0	92.0	97.5
Relative Deviation	2.41%	1.74%	2.39 %	2.09%	1.75%	3.33%	3.38%	1.83 %	1.20%	0.62%

NOTE: ‘SPT’ is the abbreviation of support base.

site loading experiment, which lays evidence for the method validation when performing deflection calculation via multiple strain measurement. The static deflection is extended by the identified support forces in concerning region, as seen in Fig. 15.

Deflection deviation by identification and extension ranges from 0.2 to 3.1 mm. Relative deviation between deflection measurement and extension calculation is within the range of 0.94~2.52%. The static deflection is the evidence for transferring the synthetic deflection into dynamic deflection in on-vehicle experiment.

IV. MONITORING AND EVALUATION

A. EXPERIMENT OVERVIEW

In-transit monitoring and evaluation was carried out during the railway freight transport from Shanhaiguan to Huade in China. Total transport distance is about 1400 km. Transformer weight and loading dimensions are the same as described in on-site loading experiment.

For well-hole freight train, a notable change of support force on load-carrying beams can be observed when the train runs on line curves, in terms of increase on one side and decrease on the other. Resulting deflections of the two beams

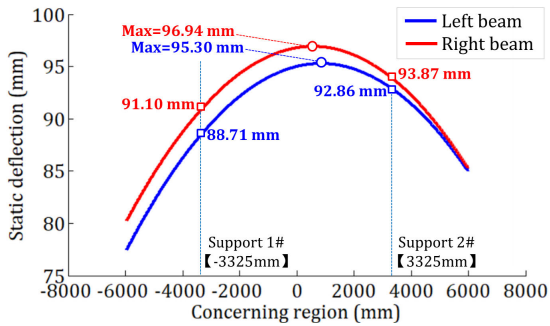


FIGURE 15. Static deflection extended by identified support loads.



FIGURE 16. The special train for transformer transport from Shanhaiguan to Huade.

TABLE 6. Speed limit on line curves of DK₃₆-type well-hole car.

Curve radius (m)	Speed limit (km/h)
≥800	60
600~800	50
400~600	40
300~400	30
260~300	20
180~260	10

follow the same rule, either positive in dynamic compression or negative in alleviation of support loads. Therefore, of all detections during the transport, only measurement on line curves is taken into account. For loaded DK₃₆-type well-hole train, defined speed limit on different curve radius are given in Table 6.

For strain measurement, strain gauges were arranged in full Wheatstone bridge, three of which are bonded on a dummy block. The material of the dummy block is the same with load-carrying beam. And its location is beside the strain measuring point, so as to compensate the environmental temperature drift. Dynamic strain signal were collected by IMC DAQ system at a sampling frequency of 256 Hz, so as to cover the main vibration frequency of loading frame, 7.4 Hz for the 1st-order vertical bending in modal analysis [52]. Before

analysis, strain data were processed with low-pass filtering at frequency of 40 Hz [53].

Running speed of freight train was detected by Stalker-S3 type velocimeter, precision of which is within ±1km/h. Running mileage, which describes the train location, is calculated with the running speed and time interval. The running mileage is consistently updated with railway mileage post to eliminate location errors. Thanks to the railway administration, information including curve radius, corresponding superelevation and mileage location are given, to analyze with monitoring results.

B. RESULTS DISCUSSION

In monitoring of bottom strains underneath load-carrying beams, the identified support forces, support deflections will be analyzed with relevant parameters, including the running speed, curve radius and superelevation. For railway line curves, the curve direction is defined the same with the centrifugal force when running forward.

Line curves scatter in different section between railway stations. Bottom strains on straight line are far lower than those on line curves. Therefore, curve-related data are intercepted from sections and spliced together. Dynamic deflection in transport is extracted from synthetic deflection, by subtraction of the static deflection measured in loading experiment. A time-history of dynamic bottom strains, synthetic support forces and synthetic support deflections are given in Fig. 17. The dynamic support deflection is calculated by the subtraction of identified synthetic and measured static support deflections. Dynamic support deflections and maximum deflection are listed in Table 7.

In assistance with the strain time-history, 3D contour map of the synthetic deflection in concerning region, are given as in Fig. 18(a) and Fig. 18(b) for the left and right beam, respectively. And dynamic deflection contour map are given in Fig. 18(c) and Fig. 18(d) for the left and right beam, respectively.

From the above monitoring and identification, the maximum detected strain of the left beam occurs on a 400-m radius line curve (superelevation: 105 mm) when the train is running at the speed of 19.6 km/h. Identified synthetic support loads and support deflections climb up to the maximum, 1286.3 kN and 135.2 mm at support 1#, 1008.1 kN and 133.7 mm at support 2#. For the right beam, the maximum strain detection arises on a 400-m radius line curve (superelevation: 105 mm) at the running speed of 17.5 km/h. Identified synthetic support loads and deflections rise up to 1232.4 kN and 130.7 mm at support 1#, and 1149.6 kN and 129.5 mm at support 2#.

Dynamic monitoring reveals that, on right line curve there is a dynamic compression on the right beam, which brings about a positive dynamic strain and deflection at support bottom. While an alleviation happens on the left beam, which arouses a negative dynamic bottom strain and deflection. The same rule follows when the train is passing through a left line curve. Results also suggest that there is an opposite trend of dynamic deflection concurrently observed between the left

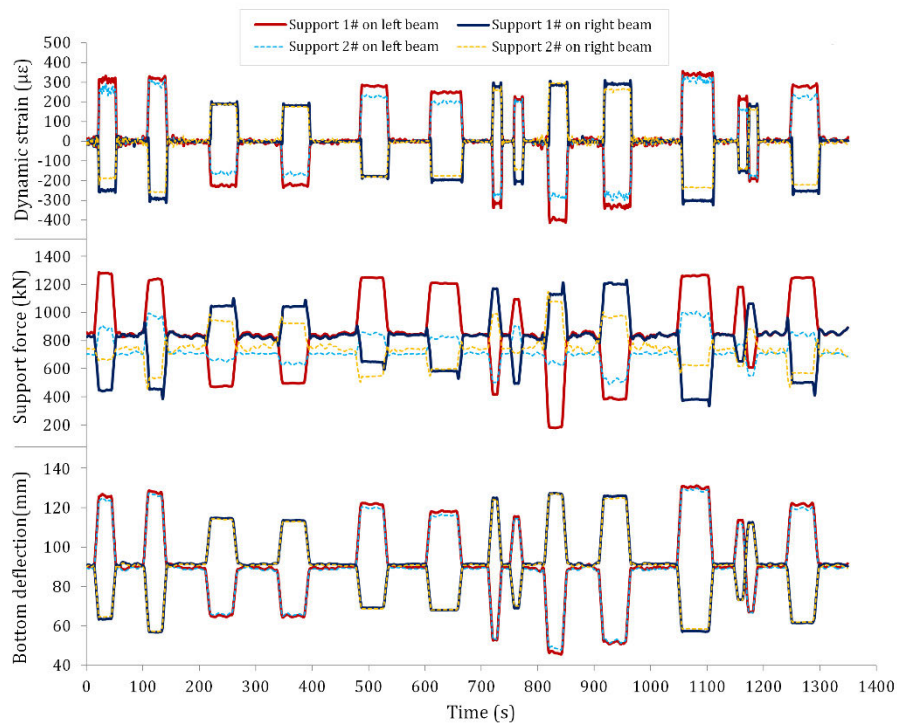


FIGURE 17. Time-history of strain detection, support load and bottom deflection identification.

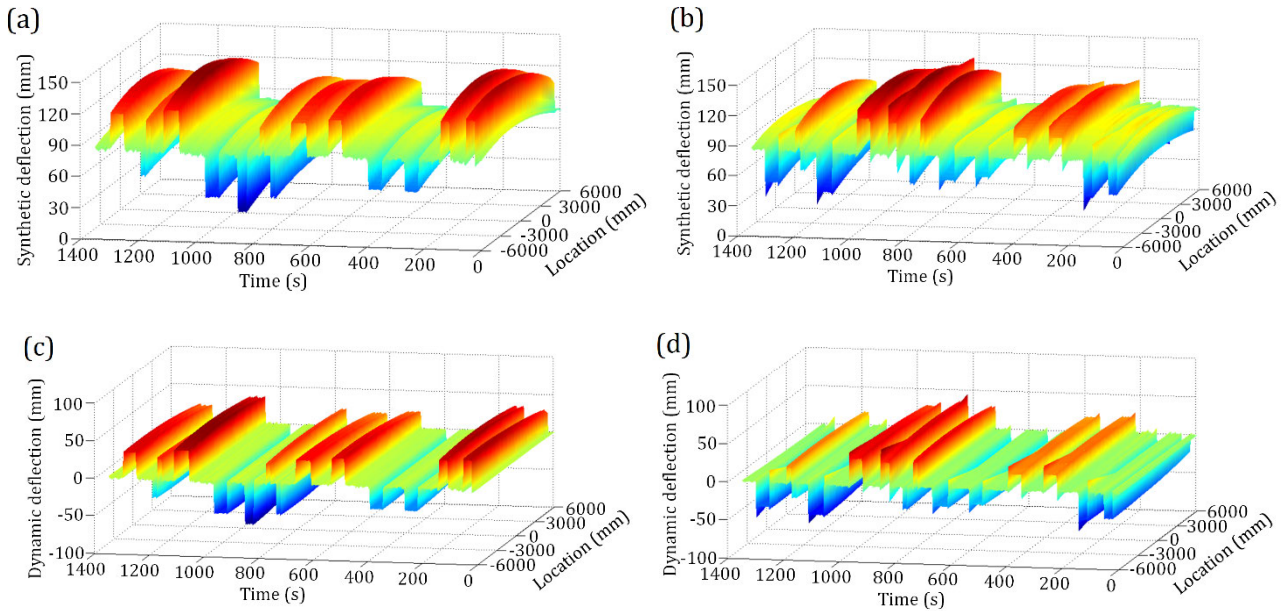
TABLE 7. Dynamic deflection on different line curves.

Curve direction	Super-elevation (mm)	Curve radius (m)	Running speed (km/h)	Deflection identification/mm					
				Left beam			Right beam		
				1#	2#	Max	1#	2#	Max
left	100	600	26	39.3	38.3	42.4	-30.1	-29.0	-33.3
left	105	600	26	40.3	39.9	42.8	-36.2	-34.9	-40.0
right	85	600	34	-25.9	-24.4	-30.9	24.5	24.2	26.1
right	100	400	35	-26.7	-25.4	-30.7	23.5	23.1	25.1
left	110	400	36	33.1	31.8	36.9	-23.2	-23.0	-24.6
left	85	600	32	29.3	28.1	32.8	-24.5	-23.7	-26.9
right	110	400	22.5	-39.6	-38.4	-43.2	36.0	35.5	38.3
left	70	800	17	27.7	27.4	29.4	-23.8	-22.1	-30.3
right	105	400	17.5	-39.5	-38.7	-42.3	37.7	37.5	40.0
right	100	400	16	-40.5	-39.4	-43.9	36.5	35.5	39.6
left	105	400	19.6	43.2	42.7	45.9	-36.1	-34.0	-43.1
left	70	800	28	25.7	24.2	30.7	-19.3	-19.0	-20.6
right	65	800	22	-24.4	-24.0	-26.0	22.7	22.2	24.4
left	85	600	17	34.2	33.0	37.7	-31.4	-30.2	-34.9
Measured static deflection				92.0	91.0	97.0	93.0	92.0	97.5

and the right beam. On left line curves, all positive dynamic deflections occur on the left beam whereas negative on the right beam. And on right line curves, all positive dynamic deflections happen on the right beam whereas negative on the left.

Explanations were introduced in a similar way as stated in [11]. Mechanical analysis of the transformer when the train is running on a right line curve is given in Fig. 19.

Taking the transformer as the analysis object, in the view of its section along width direction, the gravity force (denoted



(a) synthetic deflection of left beam; (b) synthetic deflection of right beam; (c) dynamic deflection of left beam; (d) dynamic deflection of right beam

FIGURE 18. Time-history of synthetic deflection contour map of load-carrying beams.

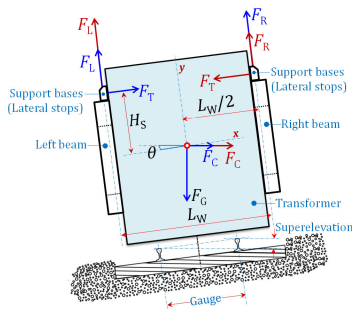


FIGURE 19. Mechanical analysis running on right line curve (blue arrows: $F_R > F_L$; red arrows: $F_L > F_R$).

as F_G) and centrifugal force (denoted as F_C) are acting at the gravity center. The supporting forces (denoted as F_L and F_R respectively for the left and right beam) are working from the 4 support bases. And the lateral forces (denoted as F_T) act from the lateral stops which only offer an inner stop force at an individual beam. When the support force F_L from the left beam is greater than that from the right beam F_R , the lateral force F_T locates from the right beam to balance the moment about the gravity center, as demonstrated with red arrows in Fig. 19. The circumstance turns out the opposite when support force F_R from the right beam exceeds that from the left beam F_L . The lateral force F_T comes from the left as the force depicted with blue arrows in Fig. 19. According to the force and moment equilibrium, the difference of support forces from the two beams is given in (20) [11].

$$F_R - F_L = 2H_S \cdot m \cdot (g \cdot \sin \theta - v^2 \cdot \cos \theta / R) / L_W \quad (20)$$

where H_S is the vertical distance between lateral force F_T and transformer gravity center. m is the mass of transformer. g is the acceleration of gravity (9.8 m/s^2), v is the running speed, R is the curve radius, θ is the curve superelevation angle.

To better understand the difference of support forces on beams, the lateral acceleration parameter is defined by J_{NRL} and calculated by $J_{NRL} = (g \cdot \sin \theta - v^2 / R \cdot \cos \theta)$. The scatter diagram of J_{NRL} vs. (v^2 / R) is given by re-calculation of running speed, curve radius and superelevation from Table 8, as in Fig. 20.

Calculations indicate that all J_{NRL} values are positive, which certifies that the supporting force from the beam at outer track side is greater than that at inner on line curves. The centrifugal force directly relates to the running speed and geometric radius of line curves. While the speed limit defined for the well-hole car, fails to create adequate centrifugal force to balance the centripetal force from the transformer gravity, but works with the lateral stops on the beam at the inner track side. In addition, the dynamic support deflections can be linearly correlated with the lateral acceleration parameter, in an approximate linear relation as seen in Fig. 21.

The fitting formulation is helpful in estimating the maximum dynamic support deflection in railway freight transport, wherein the same loading weight but different line curves and running speed are involved. The most unfavorable deflection of the transformer, locates at the transformer boundary at the tilting side rather than the support bases on the beam, when there is a difference between deflections at two support bases. But the deflection increase is no bigger than 1mm according to the calculations in [11], the deflection at support bases of load-carrying beam thus describes the most unfavorable displacement of the transformer in safety evaluation.

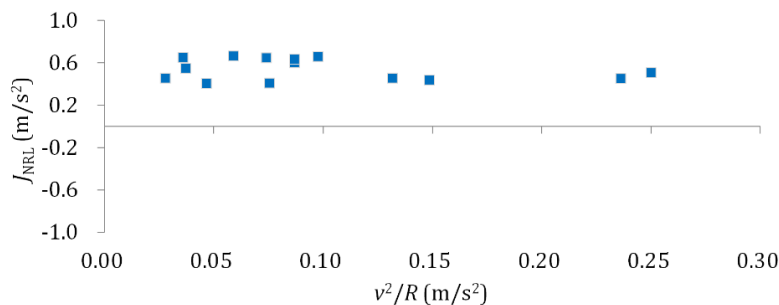


FIGURE 20. Scatter diagram of J_{NRL} vs. (v^2/R) .

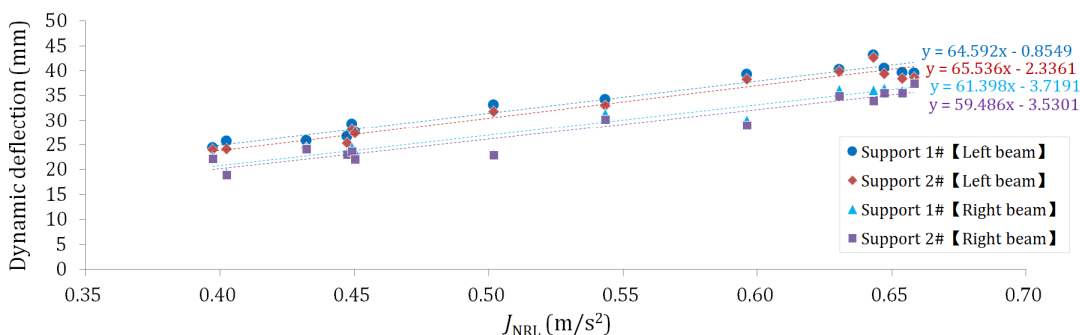


FIGURE 21. Correlation between absolute dynamic support deflections and lateral acceleration parameter.

TABLE 8. Measured displacement at suspensions and identified support deflections (mm).

Displacement measurement	Primary suspension		Second suspension		Third suspension		Total suspension		Left beam deflection		Right beam deflection	
	Left	Right	Left	Right	Left	Right	Left	Right	SPT1#	SPT2#	SPT1#	SPT2#
Static	28.0	27.6	13.2	12.8	10.8	10.6	52.0	51.0	92.0	91.0	93.0	92.0
Dynamic	21.6	18.8	12.5	10.9	10.3	9.0	44.4	38.7	43.2	42.7	37.7	37.5
Total	49.6	46.4	25.7	23.7	21.1	19.6	96.4	89.7	135.2	133.7	130.7	129.5

NOTE: ‘SPT’ is short for support base.

C. SAFETY EVALUATION

Transformer movement in vertical direction, which contains the elastic deformation of load-carrying beams and rigid displacement at suspensions, is concerned in safety evaluation. It has been discussed that the support deflections on the beam account for the most unfavorable vertical transformer movement. Thus, the maximum dynamic and synthetic deflection at support bottoms are included to assess the safety limit of 250 mm, dynamic for post-loading when the limit is measured after loading, synthetic for pre-loading when the measurement goes before loading.

Draw-wire displacement sensors (WSS-0500-D40-22V0) are set at different suspensions, serving in displacement measurement during static transformer loading, and dynamic monitoring in transit, as in Fig. 22. In measurement, six displacement sensors were set wherein two at the primary suspension of two sides of the first wheel, two at the second suspension of both sides of small frame, and the other two at the third suspension of medium frame, all in forward direction.



(a) Primary suspension, (b) second suspension, and (c) third suspension.

FIGURE 22. Installation of displacement sensors at three suspensions.

In static loading and on-vehicle transport, the displacement changes were read from the IMC DAQ system. Static, dynamic and total displacement at all suspensions, as well

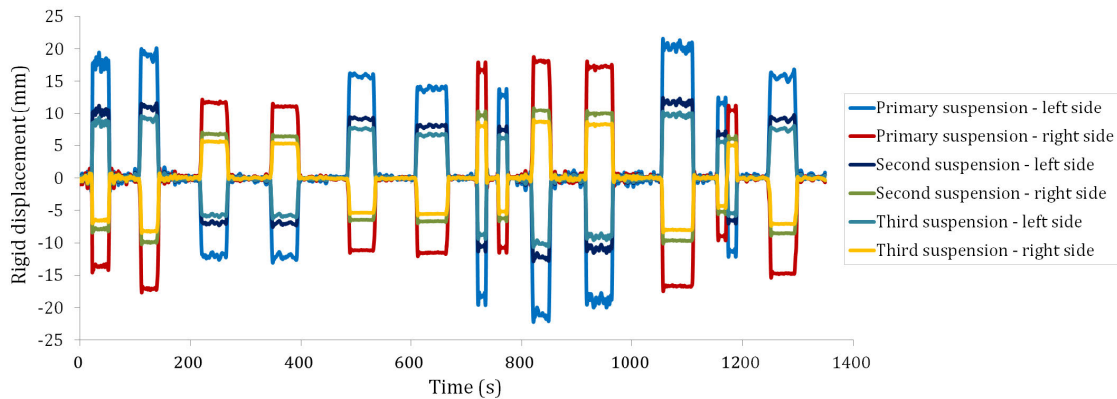


FIGURE 23. Time-history of dynamic rigid displacement at different suspensions.

as the maximum identified support deflections are listed in Table 8 and Fig. 23.

Safety evaluation undergoes in dynamic and static terms. The dynamic evaluation puts the safety limit, 250-mm space between transformer bottom and rail top, as the measured dimension after the transformer is loaded. Accordingly, the synthetic evaluation contains the limit before the transformer is loaded. Hence, according to the monitoring and calculations in Table 8, the total displacement is acquired by adding the total suspension displacement with the maximum support deflection at each side, in dynamic or synthetic way. In dynamic evaluation, the estimated total displacement reaches 87.6 mm and 76.4 mm at the left and right side, respectively. While the estimation climbs up to 231.6 mm and 220.4 mm at left and right side in synthetic evaluation. It is observed that the maximum vertical movement of the transformer does not exceed the safety limit, but pretty close to when taking account into synthetic evaluation. Therefore, it is suggested that the limit measurement be done after the transformer is loaded.

V. CONCLUSION

In this work, load identification and deflection calculation approach of opening beam on well-hole freight car is proposed. The presented model is validated by coupled loading simulation and static loading experiment, and applied in safety evaluation in transport. Conclusions derived are as follows:

(1) Support load identification is modeled by blending the mechanical relation of strain-load in single support loading with the other. Deflection calculation is formulated with the identified support loads, which takes account into different support locations in practical engineering. The proposed methodology offers a safety evaluation means for non-uniform and opening beams of well-hole freight car.

(2) Simulation validation goes in random coupled loading. Results reveal that the load deviation between identification and the given is no more than 5.98% for single beam and

loading frame, respectively. The deflection deviation between calculation and what read is no greater than 3.28%. Experiment validation reveals that the measured strains, identified support forces and deflections at support base 1#, are larger than that on support base 2#. Load deviation between identification and theoretical calculation ranges from 2.41% to 3.38%. Deflection deviation between identification and measurement ranges from 1.83% to 2.39%. Validation suggests good agreement of the proposed method with simulation and experiment.

(3) On-vehicle monitoring gives a maximum detection of $356.3\mu\epsilon$ for dynamic support bottom strains, identification of 1286.3 kN for synthetic support loads, 43.2 mm and 135.2 mm for dynamic and synthetic support deflections, respectively, when the train runs at the speed of 19.6 km/h on a 400-m line curve. It is proved both experimentally and theoretically, that the supporting force on the beam at the outer track side is greater than that at the inner, due to the speed limit defined on line curves. It also suggests that all positive dynamic deflection occurs on the left beam whereas negative on the right when running on left line curves. Same rule follows when the train is running on right line curves.

(4) In safety evaluation, the rigid displacement at all suspensions and the elastic deformation on the load-carrying beam are taken into account. With the displacement measurement via draw-wire sensors at three suspensions, the most unfavorable vertical movement of transformer rises up to 87.6 mm and 231.6 mm in dynamic and synthetic evaluation, respectively, within the range of the safety limit, 250 mm. The synthetic evaluation approximates the safety limit, it is therefore suggested that the limit dimension be measured after the transformer is loaded.

(5) Research outcome reveals the reliability and accuracy of the proposed method, and thus enables real-time deflection monitoring and safety evaluation in freight transport. In the future, the load identification model will be serving as an important part in multi-load identification, including the vertical support loads, the lateral loads and longitudinal loads from stop structures. All external loads work in cooperation

to form the real-service load spectrum of the loading frame in assistance with FEA method, so as to perform the fatigue damage estimation and structural optimization for the car.

REFERENCES

- [1] Y. Guo, "Development of high-speed railway and China rail freight transportation," *Railway Econ. Res.*, vol. 6, pp. 27–31, Jun. 2010.
- [2] Z. Xu, J. Wei, and X. Chen, "Vehicle recognition and classification method based on laser scanning point cloud data," in *Proc. Int. Conf. Transp. Inf. Saf. (ICTIS)*, Jun. 2015, pp. 44–49.
- [3] Z. Yin, C. Wu, and G. Chen, "Concrete crack detection through full-field displacement and curvature measurements by visual mark tracking: A proof-of-concept study," *Struct. Health Monit., Int. J.*, vol. 13, no. 2, pp. 205–218, Mar. 2014.
- [4] J. H. Lee, S. K. Cheong, J. S. Kim, and K. Y. Eum, "Impact characteristics and damage detection of woven carbon/epoxy laminates for car body structures of a tilting train," *Key Eng. Mater.*, vols. 321–323, pp. 942–945, Oct. 2006.
- [5] Y. Lu, T. Wang, M. Yang, and B. Qian, "The influence of reduced cross-section on pressure transients from high-speed trains intersecting in a tunnel," *J. Wind Eng. Ind. Aerodyn.*, vol. 201, Jun. 2020, Art. no. 104161, doi: 10.1016/j.jweia.2020.104161.
- [6] Y. Tao, M. Yang, B. Qian, F. Wu, and T. Wang, "Numerical and experimental study on ventilation panel models in a subway passenger compartment," *Engineering*, vol. 5, no. 2, pp. 329–336, Mar. 2019.
- [7] S. Kaewunruen, T. Ishida, and A. Remennikov, "Impact analyses for negative flexural responses (hogging) in railway prestressed concrete sleepers," *J. Phys., Conf. Ser.*, vol. 744, no. 1, Sep. 2016, Art. no. 012101.
- [8] W. Al-Nuaimy, A. Eriksen, and J. Gasgoyne, "Train-mounted GPR for high-speed rail trackbed inspection," in *Proc. 10th Int. Conf. Ground Penetrating Radar*, Feb. 2004, pp. 631–634.
- [9] S. Kaewunruen and A. M. Remennikov, "Nonlinear transient analysis of a railway concrete sleeper in a track system," *Int. J. Struct. Stability Dyn.*, vol. 8, no. 3, pp. 505–520, Sep. 2008.
- [10] S. Kaewunruen and A. M. Remennikov, "Effect of improper ballast packing/tamping on dynamic behaviors of on-track railway concrete sleeper," *Int. J. Struct. Stability Dyn.*, vol. 7, no. 1, pp. 167–177, Mar. 2007.
- [11] W. Zhou, L. Chen, T. Wang, Z. Gao, J. He, and X. Liang, "Deflection calculation and dynamic detection of non-uniform beam via multi-point strain measurement for freight trains," *IEEE Access*, vol. 7, pp. 104692–104709, 2019.
- [12] F. Yi, "Study on bridge deformation monitoring method and experiment based on FBG," M.S. thesis, Dept. Archit. Civil Eng., Suzhou Univ. Sci. Technol., Suzhou, China, 2017.
- [13] P. Li, Z. Zhang, and J. Zhang, "Simultaneously identifying displacement and strain flexibility using long-gauge fiber optic sensors," *Mech. Syst. Signal Process.*, vol. 114, pp. 54–67, Jan. 2019.
- [14] D. Adams, J. White, M. Rumsey, and C. Farrar, "Structural health monitoring of wind turbines: Method and application to a HAWT," *Wind Energy*, vol. 14, no. 4, pp. 603–623, May 2011.
- [15] H. Li, L. Zhu, G. Sun, M. Dong, and J. Qiao, "Deflection monitoring of thin-walled wing spar subjected to bending load using multi-element FBG sensors," *Optik*, vol. 164, pp. 691–700, Jul. 2018.
- [16] A. C. Pisoni, C. Santolini, D. E. Hauf, and S. Dubowsky, "Displacements in a vibrating body by strain gage measurements," *Proc. SPIE*, vol. 2460, p. 119, Jan. 2001.
- [17] G. C. Foss and H. D. Haugse, "Using modal test results to develop strain to displacement transformations," *Proc. SPIE*, vol. 2460, p. 112, Jan. 1995.
- [18] D. Geng, "Dynamic deflection estimation of beam bridges based on dynamic strain," M.S. thesis, Dept. Civil Hydraulic Eng., Hefei Univ. Technol., Hefei, China, 2015.
- [19] A. Tessler and J. L. Spangler, "A least-squares variational method for full-field reconstruction of elastic deformations in shear-deformable plates and shells," *Comput. Methods Appl. Mech. Eng.*, vol. 194, nos. 2–5, pp. 327–339, Feb. 2005.
- [20] W. Chung, S. Kim, N.-S. Kim, and H.-U. Lee, "Deflection estimation of a full scale prestressed concrete girder using long-gauge fiber optic sensors," *Construct. Building Mater.*, vol. 22, no. 3, pp. 394–401, Mar. 2008.
- [21] R. Glaser, V. Caccese, and M. Shahinpoor, "Shape monitoring of a beam structure from measured strain or curvature," *Exp. Mech.*, vol. 52, no. 6, pp. 591–606, Jul. 2012.
- [22] H. Xu and W. Ren, "Measurement of bridge deflection curve based on fiber Bragg grating sensor," in *Proc. 21th Int. Conf. SCAMI Rep.* Beijing, China: Science Press, 2007, pp. 931–935.
- [23] C. Yang, Z. Chen, Z. Wu, and W. Hong, "Research on structural deformation monitoring based on distributed fiber grating sensor," in *Proc. 4th Conf. Tech. Seminar Damage Warning Condition Assessment*, Nanjing, China, Oct. 2012, pp. 172–179.
- [24] S. Shen, Z. Wu, and Q. Yang, "An improved conjugated beam method for structural deformation on monitoring based on distributed optical fiber strain sensing technique," *China Civil Eng. J.*, vol. 7, pp. 63–70, Jul. 2010.
- [25] L.-H. Kang, D.-K. Kim, and J.-H. Han, "Estimation of dynamic structural displacements using fiber Bragg grating strain sensors," *J. Sound Vib.*, vol. 305, no. 3, pp. 534–542, Aug. 2007.
- [26] H.-I. Kim, L.-H. Kang, and J.-H. Han, "Shape estimation with distributed fiber Bragg grating sensors for rotating structures," *Smart Mater. Struct.*, vol. 20, no. 3, Mar. 2011, Art. no. 035011.
- [27] H. Jiang, B. van der Veek, D. Kirk, and H. Gutierrez, "Real-time estimation of time-varying bending modes using fiber Bragg grating sensor arrays," *AIAA J.*, vol. 51, no. 1, pp. 178–185, Jan. 2013.
- [28] S. Rapp, L.-H. Kang, J.-H. Han, U. C. Mueller, and H. Baier, "Displacement field estimation for a two-dimensional structure using fiber Bragg grating sensors," *Smart Mater. Struct.*, vol. 18, no. 2, Feb. 2009, Art. no. 025006.
- [29] J. Treiber, U. Mueller, and J.-H. Han, "Filtering techniques in the dynamic deformation estimation using multiple strains measured by FBGs," in *Proc. Conf. SPIE 15th Annu. Symp. Smart Struct. Mater. Rep.*, San Diego, CA, USA, vol. 6928, Jan. 2008, Art. no. 69322A.
- [30] C. Huang, "Strain modes identification and application for beam bridges," M.S. thesis, Dept. Archit. Civil Eng., Hefei Univ. Technol., Hefei, China, 2016.
- [31] L. Wang, Z. Wang, and D. Geng, "Strain modes based dynamic deflection estimation of continuous beam structures," *Energy Mech.*, vol. 34, pp. 142–150, Jan. 2017.
- [32] H. Fukunaga, N. Hu, and F.-K. Chang, "Structural damage identification using piezoelectric sensors," *Int. J. Solids Struct.*, vol. 39, no. 2, pp. 393–418, Jan. 2002.
- [33] K. Choi and F.-K. Chang, "Identification of impact force and location using distributed sensors," *AIAA J.*, vol. 34, no. 1, pp. 136–142, Jan. 1996.
- [34] C. Boller, C. Biemans, W. J. Staszewski, K. Worden, and G. R. Tomlinson, "Structural damage monitoring based on an actuator-sensor system," *Proc. SPIE*, vol. 3668, pp. 285–294, Jun. 1999.
- [35] W. J. Staszewski, R. B. Jenal, A. Klepka, M. Szwedo, and T. Uhl, "A review of laser Doppler vibrometry for structural health monitoring applications," *Key Eng. Mater.*, vol. 518, pp. 1–15, Jul. 2012.
- [36] J. L. Beck, S.-K. Au, and M. W. Vanik, "Monitoring structural health using a probabilistic measure," *Comput.-Aided Civil Infrastruct. Eng.*, vol. 16, no. 1, pp. 1–11, Dec. 2002.
- [37] J. Ko, K. Chak, and J. Wang, "Formulation of an uncertainty model relating modal parameters and environmental factors by using long-term monitoring data," *Proc. SPIE*, vol. 5057, pp. 298–307, Aug. 2003.
- [38] S. Jamali, T. H. T. Chan, K.-Y. Koo, A. Nguyen, and D. P. Thambiratnam, "Capacity estimation of beam-like structures using substructural method," *Int. J. Struct. Stability Dyn.*, vol. 18, no. 12, Dec. 2018, Art. no. 1850162.
- [39] F. Liu, S. Gao, H. Han, Z. Tian, and P. Liu, "Interference reduction of high-energy noise for modal parameter identification of offshore wind turbines based on iterative signal extraction," *Ocean Eng.*, vol. 183, pp. 372–383, Jul. 2019.
- [40] N. T. Chowdhury, W. K. Chiu, and J. Wang, "Biaxial specimen design for structures subjected to multi-axial loads," *Adv. Mater. Res.*, vols. 891–892, pp. 1633–1638, Mar. 2014.
- [41] S. L. Lee, C. G. Koh, and C. David, "Vibration and performance of a subway track system based on the third y K Cheung lecture," *Dental Mater. Off. Publication Acad. Dental Mater.*, vol. 27, no. 9, pp. 948–953, Mar. 2011.
- [42] P. Lively, "Dynamic structural shape estimation using integral sensor arrays," M.S. thesis, Dept. Aeronaut. Astronaut. Eng., Massachusetts Inst. Technol., Cambridge, MA, USA, 2000.
- [43] Z.-W. Chen, Q.-L. Cai, and S. Zhu, "Damage quantification of beam structures using deflection influence lines," *Struct. Control Health Monitor.*, vol. 25, no. 11, Nov. 2018, Art. no. e2242.
- [44] X. Qi, "Dynamic deflection characteristics prediction and experimental analysis on the beam structure," M.S. thesis, Dept. Mechatronic Eng., Beijing Jiaotong Univ., Beijing, China, 2012.

- [45] X. R. Yuan, "Calculating the dynamic deflection from bridge measuring acceleration," *J. Guangzhou Univ. (Natural Sci. Ed.)*, vol. 1, pp. 75–78, Jan. 2007.
- [46] J. Keenahan, E. J. O'Brien, P. J. McGetrick, and A. Gonzalez, "The use of a dynamic truck-trailer drive-by system to monitor bridge damping," *Struct. Health Monit., Int. J.*, vol. 13, no. 2, pp. 143–157, Mar. 2014.
- [47] S. Chen, F. Cerda, J. Guo, J. B. Harley, Q. Shi, P. Rizzo, J. Bielak, J. H. Garrett, and J. Kovacevic, "Multiresolution classification with semi-supervised learning for indirect bridge structural health monitoring," in *Proc. IEEE Int. Conf. Acoust., Speech Signal Process.*, May 2013, pp. 3412–3416.
- [48] D. Adams, *Health Monitoring of Structural Materials and Components: Methods With Applications*. Hoboken, NJ, USA: Wiley, 2007.
- [49] C. J. L. Cowled, D. P. Thambiratnam, T. H. T. Chan, and A. C. C. Tan, "Structural complexity in structural health monitoring: Design of laboratory model and test plan," in *Proc. 7th World Congr. Eng. Asset Manage. (WCEAM)*, Oct. 2012, pp. 171–181.
- [50] C. J. L. Cowled, D. P. Thambiratnam, T. H. T. Chan, and A. C. C. Tan, "Structural complexity in structural health monitoring: Preliminary experimental modal testing and analysis," in *Proc. 7th World Congr. Eng. Asset Manage. (WCEAM)* Oct. 2012, pp. 183–193.
- [51] G. Zhang, G. Guo, L. Li, and C. Yu, "Study on the dynamic properties of a suspended bridge using monocular digital photography to monitor the bridge dynamic deformation," *J. Civil Struct. Health Monitor.*, vol. 8, no. 4, pp. 555–567, Sep. 2018.
- [52] A. Guo, "Fatigue assessment and monitoring scheme optimization of well car frame structure based on service load," M.S. thesis, Dept. Traffic Transp. Eng., Central South Univ., Hunan, China, 2018.
- [53] *Regulations on Dynamic Performance Evaluation and Test Appraisal for Rolling Stock*, Standard GB/T 5599-2019, Standard Press, Beijing, China, 2019.



LIN CHEN is currently pursuing the master's degree with the School of Traffic and Transportation Engineering, Central South University, Changsha, China. Her major interest is vehicle operation engineering and her research interest includes railway freight transport safety monitoring and evaluation.



JIE HE received the master's degree from the School of Traffic and Transportation, Beijing Jiaotong University, Beijing, China, in 2005. He is currently the Deputy Chief of China State Railway Group Company Ltd. His research interests include railway out-of-gauge freight transport and railway construction clearance management.



YITONG WU is currently pursuing the master's degree with the School of Traffic and Transportation Engineering, Central South University, Changsha, China. Her major interest is vehicle operation engineering and her research interests include safety monitoring and evaluation of railway freight transport.



XIFENG LIANG received the bachelor's and the master's degrees from the School of Energy and Environment Engineering, Southeast University, Nanjing, China, in 1985 and 1988, respectively. He is currently a Professor with Central South University. His research interest includes train operating safety and environment, especially in structural safety evaluation.



WEI ZHOU received the master's and Ph.D. degrees from the School of Traffic and Transportation Engineering, Central South University, Changsha, China, in 2007 and 2012, respectively. He is currently an Associate Professor with Central South University. His research interest includes railway freight transport safety evaluation, especially in structural health monitoring.



XIWEN GUO received the bachelor's degree from the School of Mechanical Engineering, Gezhouba Hydropower Engineering College, Yichang, China, in 1988, and the master's degree from the School of Business, Central South University, Changsha, China, in 2004. He is currently the General Manager of China Special Article Logistics Corporation Ltd. His research interest includes out-of-gauge freight transport, especially in loading reinforcement technology.



QIANXUAN WANG received the master's and Ph.D. degrees from the School of Traffic and Transportation Engineering, Central South University, Changsha, China, in 2009 and 2014, respectively. He is currently an Associate Professor with the School of Rail Transportation, Wuyi University, China. His research interests include traffic safety and railway foreign objects detecting.